Isolation, characterization, crystal structure, free radical scavenging- and computational studies of 9-[4-(propan-2-yl)phenyl]-3,4,5,6,7,9-hexahydro-1 H -xanthene-1,8(2 H)-dione...

Article *in* Journal of Molecular Structure · May 2017

DOI: 10.1016/j.molstruc.2017.05.026

8 authors, including:

Jerry P. Jasinski
Keene State College

Yusuf Yilmaz
Gaziantep University

Olatomide Fadare
Obafemi Awolowo University

Craig Obafemi
Obafemi Awolowo University

Isolation, characterization, crystal structure, free radical scavenging- and computational studies of...

Article *in* Journal of Molecular Structure · May 2017

8 authors, including:

Jerry P. Jasinski
Keene State College

Kayode Sanusi
Obafemi Awolowo University

Ümit Ceylan
Giresun University

Olatomide Fadare
Obafemi Awolowo University

Journal of Molecular Structure 1144 (2017) 396–405

Contents lists available at ScienceDirect

Journal of Molecular Structure

journal homepage: http://www.elsevier.com/locate/molstruc

Isolation, characterization, crystal structure, free radical scavenging- and computational studies of 9-[4-(propan-2-yl)phenyl]-3,4,5,6,7,9-hexahydro-1*H*-xanthene-1,8(2*H*)-dione from *Garcinia kola* seeds

Rachael Y. Agunbiade [a], Jerry P. Jasinski [b], Sean P. Millikan [b], Kayode Sanusi [a], Yusuf Yilmaz [c], Ümit Ceylan [d], Olatomide A. Fadare [a], Craig A. Obafemi [a, *]

[a] Department of Chemistry, Faculty of Science, Obafemi Awolowo University, Ile-Ife, Nigeria
[b] Department of Chemistry, Keene State College, 229 Main Street, Keene, NH, 03435-2001, USA
[c] NT Vocational School, Gaziantep University, 27310, Gaziantep, Turkey
[d] Department of Medical Services and Techniques, Vocational High School Health Services, Giresun University, 28100, Giresun, Turkey

ARTICLE INFO

Article history:
Received 26 February 2017
Received in revised form
29 April 2017
Accepted 10 May 2017
Available online 13 May 2017

Keywords:
Garcinia kola, Heckel (Guttiferae)
Xanthene-1,8(2*H*)-dione
Scavenging activity
DFT calculations
Crystal structure
Spectroscopy

ABSTRACT

A new crystallographic form of a pure xanthenedione derivative (**11′**), $C_{22}H_{24}O_3$, was isolated from the hexane extract of the seeds of *Garcinia kola*. The structure of the compound was determined on the basis of FTIR and NMR spectroscopy and confirmed by single-crystal X-ray diffraction analysis. The compound crystallized as $C_{22}H_{24}O_3$ H_2O H_3O^+ Cl^-, as the result of the extraction process, adopts monoclinic, space group P21/n (no. 14) and is stabilized by OW—H···OW, OW—H···Cl, C—H···OW, C—H···Cl intramolecular hydrogen bonds and weak OW—H···O, C—H···O, intermolecular interactions forming a 3-D supramolecular structure. The molecular property of the pure xanthene derivative, $C_{22}H_{24}O_3$, has also been investigated using the density functional theory (DFT) method. The calculated IR, ^1H and ^{13}C data were found to be in good agreement with experimental values. The compound $C_{22}H_{24}O_3$ showed weak DPPH radical scavenging activity with IC_{50} value of 2.37 ± 0.08 mg/ml.

1. Introduction

Garcinia kola, Heckel (Guttiferae) known as Bitter kola is widely distributed throughout west and central Africa. The people of this region highly value the seed for its edibility [1]. Different parts of the plant are often used in folklore medicine and herbal preparations [2] in the treatment of various diseases such as bronchitis, diarrhea, high fever gonorrhea, hepatitis, jaundice, laryngitis and liver disorders [3,4], stomach ache and gastritis [5], chest colds, colic, cough, headache [6] and so on.

The extracts of the seed have been studied and shown to have several pharmacological effects such as antimicrobial [7,8], analgesic, anti-inflammatory, antipyretic [9,10], antimalarial [11], antioxidant [12,13], cancer chemopreventive [14], anti-diabetic [15], molluscicidal [16], anti-atherogenic [17], aphrodisiac [18], hypoglycemic [19–21], and anti-degenerative arthritis [22] activities.

It is well known that the genus *Garcinia* (of the Guttiferae family) is a rich source of poly-isoprenylated benzophenones (e.g. guttiferone I (**1**)) and xanthones (e.g. garcim-2 (**2**)) (see Fig. 1) and many of them have been shown to exhibit various biological activities such as cytotoxic activity in *in vitro* and *in vivo* assay [23,24], antiplasmodial [25], antibacterial [26,27], antifungal [28], anti-inflammatory [29,30], antioxidant [24,31] and apoptosis-inducing [24] properties.

Previous phytochemical studies of the seeds of *Garcinia kola* have resulted in the isolation of triterpenes, benzophenones and phenolic compounds, including some chromanols: garcinal (**3**), garcinoic acid (**4**), δ-tocotrienol (**5**), biflavonoids: garcinianin (**6**), GB-1 (**7**), GB-2 (**8**), kolaflavanone (**9**) [32] and naringin-7-rhamnoglucoside (**10**) [33] (see Fig. 2).

Xanthenedione derivatives are not very common in nature and no xanthene-1,8-dione has been reported to be isolated from plant sources, but they are considered to be very valuable molecules because of their varied pharmacological properties [34]. However, the compound $C_{22}H_{24}O_3$ has been synthesized in the laboratory and its crystal structure reported [35]. It crystallizes in the orthorhombic

* Corresponding author.
E-mail address: craigobafemi@gmail.com (C.A. Obafemi).

http://dx.doi.org/10.1016/j.molstruc.2017.05.026
0022-2860/

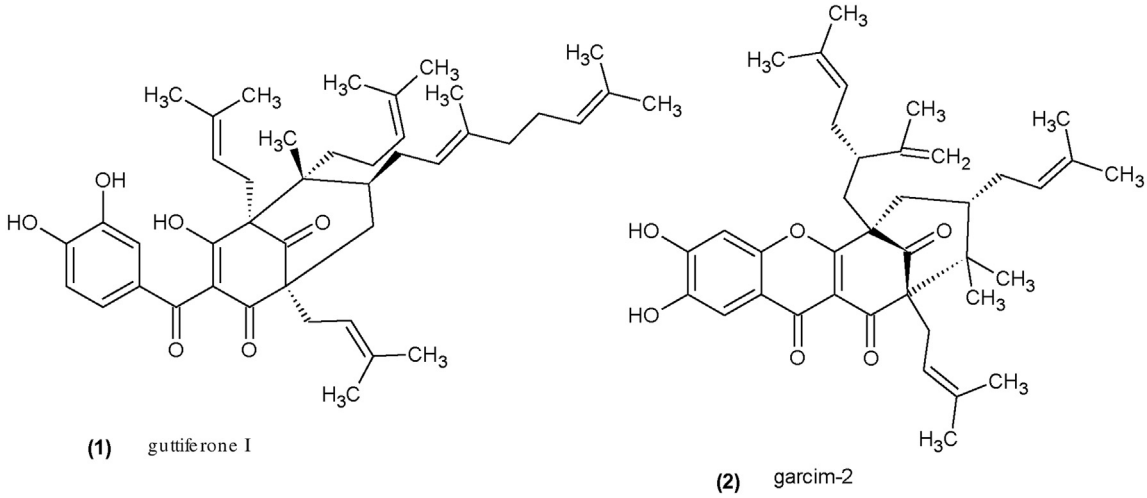

Fig. 1. Typical poly-isoprenylated benzophenone and xanthone found in genus *Garcinia.*

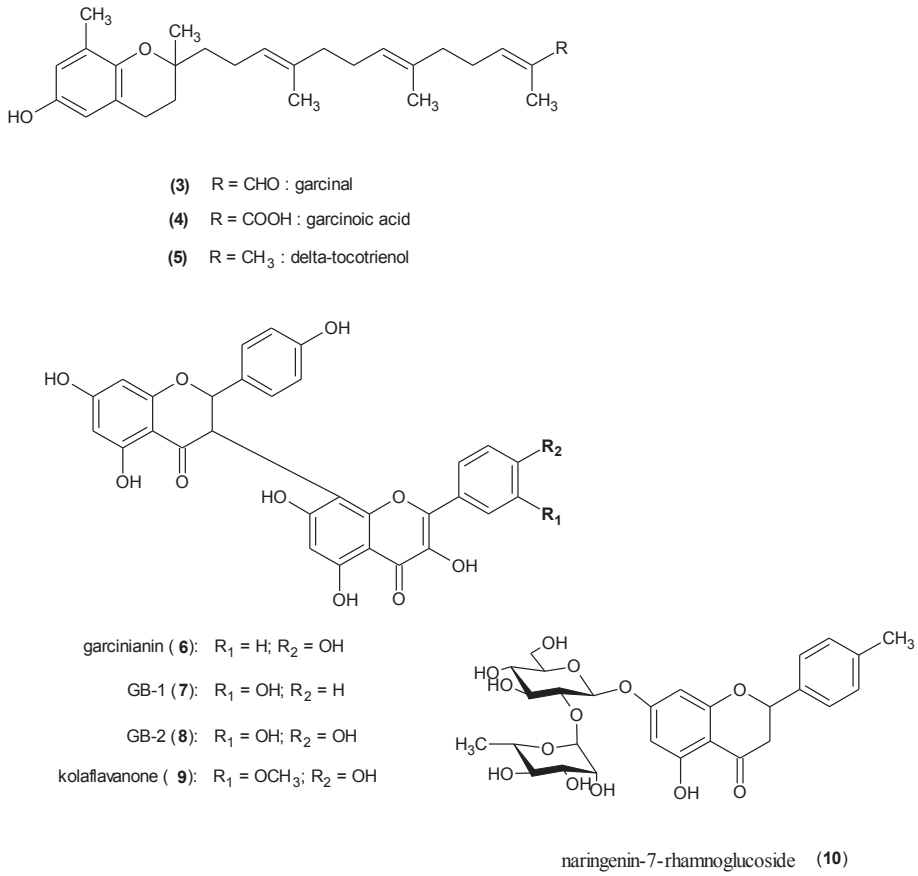

Fig. 2. Structures of reported isolated compounds from the seeds of Garcinia kola.

space group *Pnma* (No. 62) with cell dimensions a = 12.306(8) Å, b = 14.914(12) Å, c = 10.174(7) Å, $\alpha = \beta = \gamma = 90.0°$. In the present paper, we report the isolation and spectroscopic characterization, single crystal X-ray structure of the recrystallized extracted xanthenedione compound $C_{22}H_{24}O_3$ H_2O H_3O^+ Cl^-, (**11′**) and DFT calculation of the pure xanthenedione compound, $C_{22}H_{24}O_3$, (**11**) from the seeds of *Garcinia kola*. It crystallizes in the monoclinic space group, P 2_1/n (No. 14) with cell dimensions a = 11.9644(3) Å, b = 14.4534(3) Å, c = 12.8366(4) Å, $\beta = 108.424(3)^o$. We also report on the DPPH radical scavenging activity of the crude hexane extract of seeds of *Garcinia kola* and one of its fractions, in comparison to the isolated xanthenedione compound.

2. Materials and method

2.1. Materials and measurements

The *Garcinia kola* seeds were obtained locally in Ile-Ife, Nigeria

and taxonomically identified at the University Herbarium, Botany Department, Obafemi Awolowo University, Ile-Ife. The melting point was determined with an open-ended capillary tube on a Gallenkamp (variable heater) melting point apparatus and is uncorrected. Fourier transform infrared spectra were recorded on an Agilent Cary 680 spectrophotometer, equipped with a diamond tipped ATR accessory in the spectral range 4000–550 cm^{-1}, while NMR spectra were obtained with Agilent 400 MHz spectrometer, operating at 400 MHz (for ^1H NMR, delta in ppm relative to Me4Si) and 100 MHz (for ^{13}C NMR). The elemental analysis (C, H) of the compound was performed using a Carlo Erba-1108 elemental analyzer. Results were found to be in good agreement with the calculated value. Solvents used were of analytical grade and used without further purification.

2.2. Extraction and isolation

The seeds were thoroughly washed in distilled water and then dried in a Gallenkamp drying oven at 40 °C, followed by peeling. The dried and peeled seeds (1.9 kg) were pulverised by a mechanical grinder and extracted twice with 2.5 L of n-hexane in a glass jar at room temperature for 48 h, with intermittent shaking. The clear filtrate obtained after filteration was concentrated under reduced pressure to obtain the crude n-hexane extract (16.1 g). The hexane extract was subjected to column chromatography eluting with petroleum ether, petroleum ether-ethyl acetate, in increasing order of polarity. Thin layer chromatography (TLC) was used to monitor the separation and eluates with the same TLC profile were bulked and concentrated to obtain different fractions.

One of the fractions eluted with petroleum ether-ethyl acetate (10:1) (Fraction 11) was concentrated to dryness to give compound (**11**) as colorless crystals (0.5 g). Recrystallization from 95% ethanol containing concentrated hydrochloric acid with slow evaporation afforded pure colorless needles of **11′**, suitable for X-ray analysis; m.p. 169–171 °C (dec.). IR (FT-ATR; cm^{-1}): 3443, 2956, 2931, 2854, 1666, 1612, 1464, 1381, 1062 cm^{-1}. ^1H NMR ($CDCl_3$, 400 MHz) δ: 7.18 (2H, d, $J = 8.3$ Hz, aromatic), 7.05 (2H, d, $J = 8.2$ Hz, aromatic), 4.78 (1H, s, CH), 2.78–2.85 (1H, m, CH), 2.58–2.70 (4H, m, 2 × CH_2), 2.35–2.46 (4H, m, 2 × CH_2), 1.97–2.05 (4H, m, 2 × CH_2), 1.18 (6H, d, 2 × CH_3). ^{13}C NMR ($CDCl_3$, 100 MHz), δ: 20.3 (CH_2), 23.9 (CH_3), 27.2 (CH_2), 31.3 (C-9 CH), 33.6 (CH), 37.0 (CH_2), 116.9 (C_q), 126.4 (CH), 128.1 (CH), 146.5 (C_q), 164.0 (C_q), 196.8 (C=O) ppm.

2.3. Solution and refinement of the crystal structures

Single crystals of $C_{22}H_{29}O_5Cl$ (**11′**) were obtained by slow evaporation of the compound in aqueous ethanol and a concentrated HCl solution. A suitable crystal was selected and placed on a Nylon Loop on an Rigaku-Oxford Diffraction, Eos, Gemini diffractometer. The crystal was kept at 173(2) K during data collection. Using Olex2 [36], the structure was solved with the Superflip [37] structure solution program using Charge Flipping and refined with the ShelXL [38] refinement package using Least Squares minimization.

Crystal Data for **(11′)**, $C_{22}H_{29}O_5Cl$ ($M = 407.89$), monoclinic, space group $P2_1/n$ (no. 14), $a = 11.9655(3)$ Å, $b = 14.4534(3)$ Å, $c = 12.8366(4)$ Å, $\beta = 108.424(3)°$, $V = 2106.21(10)$ $Å^3$, $Z = 4$, $T = 173(2)$ K, μ(Mo Kα) = 0.211 mm^{-1}, $Dcalc = 1.286$ g/mm^3, 25892 reflections measured ($6.294 \leq 2\Theta \leq 65.812$), 7178 unique ($R_{int} = 0.0302$) which were used in all calculations. The final R_1 was 0.0519 ($I > 2\sigma(I)$) and wR_2 was 0.1647 (all data). Selected crystallographic data are presented in Table 1.

2.4. Antioxidant activity

2.4.1. DPPH radical scavenging activity

The antioxidant activity of the isolated compound, in comparison to the crude hexane extract and fraction 10, were determined using the 1,1-diphenyl-2-picrylhydrazyl (DPPH) free radical scavenging assay method, as described by Chen and Ho [39]. A DPPH solution in absolute ethanol (0.1 mM) was prepared. Also, solutions of each of the isolated compound, hexane extract and fraction 10 in absolute ethanol at different concentrations (7.813–1000 μg/ml) were prepared. 2 mL of the freshly prepared DPPH solution was mixed with 2 mL of the different solutions at different concentrations and the resulting mixtures were vortexed thoroughly, incubated in the dark for 30 min and the absorbance measured against a blank at 517 nm using a Shimadzu UV/Vis 1601 apparatus. The ability of the tested samples to scavenge DPPH radical was calculated using the following equation:

$$\textit{DPPH radical scavenging activity}\ (\%) = \left(1 - \frac{\textit{Absorbance DPPH + sample}}{\textit{Absorbance DPPH}}\right) x\ 100$$

Ascorbic acid was used as a positive control in the experiment. Values are reported as mean ± standard error of triplicate determinations.

2.5. Computational details and methods of calculation

All calculations on the molecule (**11**) were performed in gas phase using the Gaussian 03W program suite [40]. The stationary points on the potential energy surface (PES) were optimized by the density functional theory (DFT) method, with Becke three-parameter hybrid and Lee-Yang-Parr (B3LYP) correlation functional approximations [41,42]. Basis sets with increasing size in the order of the sequence 6-31G, 6-311G, 6–311++G, 6–311++G(d,p), cc-pVDZ, LanL2DZ, and SDD [43–47] were used separately for geometry optimization, with the first initial guess structure obtained via a 6-31G basis set. To achieve low computational cost in the

Table 1
Selected Crystal data and structure refinement for **(11′)**, $C_{22}H_{24}O_3$ H_2O H_3O^+ Cl^-.

Identification code	OBA (11′)
Empirical formula	$C_{22}H_{29}O_5Cl$
Formula weight	408.90
Temperature/K	173(2)
Crystal system	monoclinic
Space group	$P2_1/n$
a/Å	11.9655(3)
b/Å	14.4534(3)
c/Å	12.8366(4)
α/°	90
β/°	108.424(3)
γ/°	90
Volume/$Å^3$	2106.21(10)
Z	4
ρ calc mg/mm^3	1.290
μ/mm^{-1}	0.211
F(000)	872.0
Crystal size/mm^3	0.24 × 0.12 × 0.08
2Θ range for data collection	6.294–65.812°
Index ranges	$-18 \leq h \leq 18$, $-20 \leq k \leq 21$, $-17 \leq l \leq 18$
Reflections collected	25892
Independent reflections	7178 [R(int) = 0.0302]
Data/restraints/parameters	7178/1/265
Goodness-of-fit on F2	1.035
Final R indexes [I>=2σ (I)]	R1 = 0.0519, wR2 = 0.1499
Final R indexes [all data]	R1 = 0.0703, wR2 = 0.1647
Largest diff. peak/hole/e $Å^{-3}$	1.07/-0.47

higher-level basis for geometry optimizations, the result from a lower basis was used as the starting geometry for the higher-level calculation (e.g. the result of 6-311G was employed as the starting geometry for 6–311++G and etc.). A H_2O molecule, H_3O^+ and Cl^- ions found in the crystallography data were not included in the optimization. These molecule and ions were introduced during the re-crystallization process to obtain crystals suitable for x-ray analysis. The bond lengths obtained for each optimization method were compared pair-wisely to the X-ray crystallography data. The atom labels on the crystal and the computed structures were carefully matched to avoid mis-matching of bonds (Table 1S (see Supplementary data)).

The absolute difference between the X-ray and the calculated bond lengths and the sum of it, $\delta_{M(SUM)}$, were obtained according to Equation (1):

$$\delta_{M(SUM)} = \sum \left| BL_{X-ray_{ij}} - BL_{M_{ij}} \right| \quad (1)$$

where $BL_{X-ray_{ij}}$ represents the X-ray determined bond length of $atom_i - atom_j$, while $BL_{M_{ij}}$ denotes the calculated bond length corresponding to $atom_i - atom_j$. The subscript M in $\delta_{M(SUM)}$ and $BL_{M_{ij}}$ indicates the particular basis set employed in the optimization. The total energies of the molecule as given by the basis set M (E_M) were plotted against the $\delta_{M(SUM)}$ corresponding to M to show the energy gradient per basis.

The minimization coefficient per basis (μ_M) was calculated using Equation (2):

$$\mu_M = |E_M| \Big/ \delta_{M(SUM)} \quad (2)$$

Subsequent calculations, including the vibrational frequencies, time-dependent self-consistent field (TD-SCF), for $N = 20$ states, were performed at the cc-pVDZ level. ^1H and ^{13}C NMR, using the Gauge Independent Atomic Orbital (GIAO) method [48,49], were obtained at the B3LYP/6-31G//B3LYP/cc-pVDZ level. The frequency data allowed us to classify the optimized structure as a local minimum or transition state, and to generate the infra-red (IR) absorption data (Table 4). The TD SCF was carried out to understand the electronic absorption behavior of the molecule within 20 electronic states.

3. Results and discussion

The seeds of *Garcinia kola* were extracted with n-hexane. Silica gel column chromatography of the hexane extract yielded compound (**11**) as the main constituent from fraction 11. (**11**) contains a hexahydroxanthene ring, two keto groups, with an unusual 4-isopropylphenyl group at the C-9 position. A crystal of the compound suitable for x-ray analysis was obtained in a crystalline form as (**11′**) (Fig. 3) and completely characterized.

3.1. Spectroscopic property

In (**11**), the infrared absorption bands at 2956, 2931 and 2854 cm^{-1} are related to the stretching modes of the alkyl fragment, while the strong band at 1666 cm^{-1} showed the presence of a conjugated ketone functional group. The bands at 1612 and 1062 cm^{-1} correspond to the C=C stretching vibration and –C-O-C- structural feature in the compound, respectively.

The ^1H NMR spectrum showed a multiplet at δ 2.78–2.85 ppm integrating for 1H assigned to the methine proton of the isopropyl group, while a doublet integrating for 6H at δ 1.18 ppm corresponded to the remaining hydrogen atoms of the isopropyl group. The chemical shift of the methine proton on C-9 of the xanthene ring appeared δ 4.78 ppm. The signals for the methylene groups were observed as 4H multiplets centered at δ 2.64, 2.40 and 2.01, respectively. ^{13}C NMR of (**11**) showed a characteristic signal at δ_C 196.8 ppm for carbonyl group and 116.9–164.0 ppm for aromatic and alkenyl carbons, while the signal for the methine carbon of the isopropyl group appeared at δ 33.6 ppm and the two methyl groups at δ 23.9 ppm [50].

3.2. Crystal structure analysis of 3,4,6,7-tetrahydro-9-(4-isopropylphenyl)-2H-xanthene-1,8(5H,9H)-dione aqua hydrochloride, (11′), $C_{22}H_{24}O_3$ H_2O H_3O^+ Cl^-

Compound (**11′**) was crystallized using aqueous ethanol (95%) and concentrated HCl under slow evaporation and has been characterized by single crystal X-ray diffraction studies. An ORTEP view of the compound (showing the labeled atoms) is shown in Fig. 4A, and its packing diagram viewed along the c-direction is shown in Fig. 5. The crystallographic data and structural refinement details for compound (**11′**) are listed in Table 1. Systematic reflection conditions and statistical tests of the collected data indicate that the compound crystallized as $\mathbf{C_{22}H_{24}O_3\ H_2O\ H_3O^+\ Cl^-}$. The two 6-membered carbon rings in the xanthane-1,8(2H)-dione group fused to the central pyran group are puckered with slightly distorted envelope conformations (Q = 0.4625(18), θ = 124.9(2)°, ϕ = 314.4(2)°, C1–C6; Q = 0.4718(17), θ = 59.51(19)°, ϕ = 174.1(2)°, C8–C13) [51]. The central pyran group is puckered in a slightly

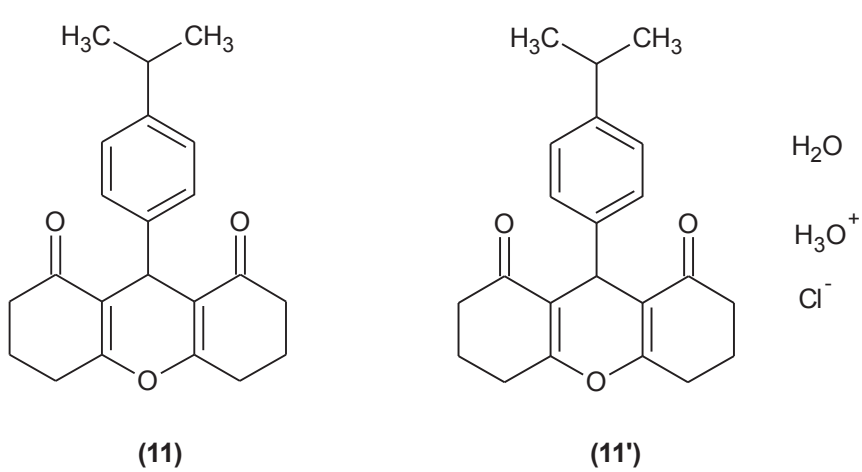

Fig. 3. Molecular structures of the isolated xanthenedione (11) and its recrystallized form (**11′**).

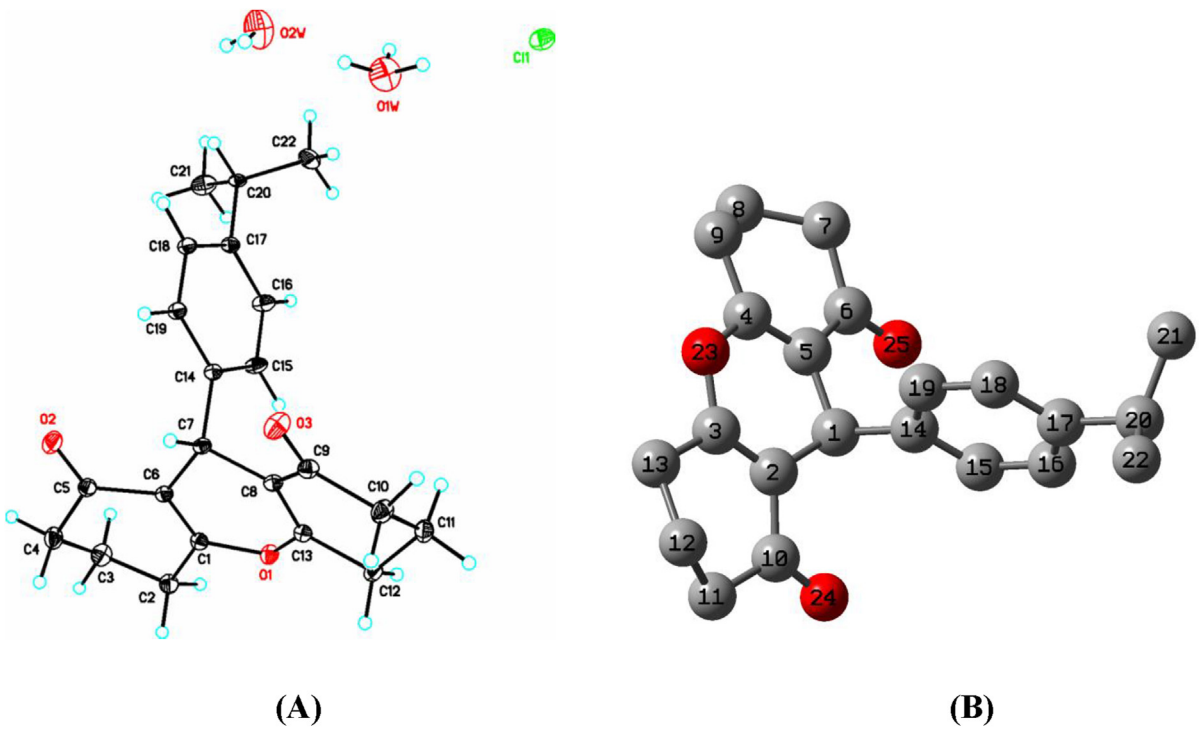

Fig. 4. (A) ORTEP drawing of (**11′**), $C_{22}H_{24}O_3$ H_2O H_3O^+ Cl^-, showing the atom numbering scheme and 30% displacement ellipsoids of non H-atoms and (B) Computational structure drawing for (11), $C_{22}H_{24}O_3$, showing the non-hydrogen atoms.

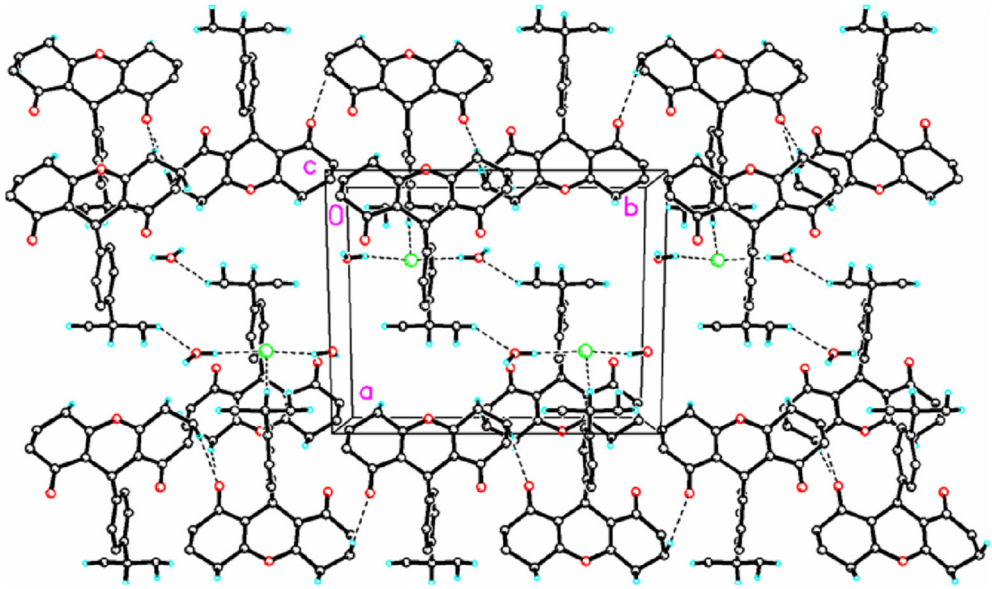

Fig. 5. The molecular packing of (**11′**), $C_{22}H_{24}O_3$ H_2O H_3O^+ Cl^-, viewed along the c axis. Dashed lines indicate OW–H···OW, OW–H···Cl, C–H···OW, C–H···Cl intramolecular hydrogen bonds and weak OW–H···O, C–H···O, intermolecular interactions forming a 3-D supramolecular structure. Hydrogen atoms not involved in hydrogen bonding have been removed for clarity.

distorted boat conformation (Q = 0.2714(14), θ = 81.3(3)°, ϕ = 178.9(3)°, O1/C1/C6/C7/C8/C13) [51]. The dihedral angle between the mean planes of the phenyl and pyran groups is 89.2(7)°. Bond lengths and angles are in normal ranges [52] and similar to those observed in the previously reported structure of $C_{22}H_{24}O_3$ [35].

The molecular packing of $C_{22}H_{24}O_3$ H_2O H_3O^+ Cl^- shows that two molecules of (**11′**) are joined together by weak C–H···O intermolecular interactions between C=O (carbonyl) and nearby C–H groups (Table 2, Fig. 5). Additional weak OW–H···O intermolecular interactions are observed between the water molecule and a carbonyl group and between the chloride ion and nearby C–H groups along with some weak C–H ··· π intermolecular interactions as well. Also, a number of intramolecular hydrogen bonds and weak intermolecular interactions between the water and hydronium ion groups themselves and with carbonyl and chloride groups as well are observed and all together form a 3-D supramolecular structure (Table 2, Fig. 5).

Table 2
Hydrogen bond and weak intermolecular interactions for (**11′**), $C_{22}H_{24}O_3$ H_2O H_3O^+ Cl^-. [Å and °].

D–H ··· A	d(D-H)	d(H ··· A)	D(D ··· A)	<(DHA)	
C2–H2B··· O3 #1	0.99	2.58	3.2520(18)	124.7	4_676
C11–H11B···O2 #2	0.99	2.57	3.429(2)	144.8	2_645
C12–H12A ··· O2 #1	0.99	2.42	3.3421(19)	154.3	4_676
C20–H20···Cl1 #3	1.00	2.06	3.0556(13)	172.3	2
C21–H21C···O2W #3	0.98	2.71	3.417(3)	129.7	2
C22–H22A ··· O1W #2	0.98	2.42	3.299(3)	149.0.	
C22–H22B···O2 #4	0.98	2.56	3.422(2)	147.0	4_576
O1W–H1WB···Cl1	0.87	2.34	3.2001(18)	169.3.	
O1W–H1WC···O2W	0.947(19)	1.913(19)	2.858(3)	175(4).	
O2W–H2WA ··· O3 #5	0.85	2.11	2.930(2)	162.0	3_665
O2W–H2WB···Cl1	0.85	2.39	3.2101(16)	161.8 2	
C4–H4A ··· Cg4	0.95	2.68	3.5175(16)	142	
C10–H10B ··· Cg4	0.96	2.87	3.7651(16)	151	

Symmetry codes: #1 ½+x,3/2−y,1/2 + z; #2 3/2−x,−1/2 + y,1/2−z; #3 1/2−x, 1/2 + y,1/2−z; #4 −1/2 + x, 3/2−y, 1/2 + z; #5 1−x, 1−y, −z; Cg4 = C14–C19.

3.3. Antioxidant activity

The free radical scavenging activity of the isolated xanthenedione, **11′**, the crude hexane extract and fraction 10, was evaluated using an ethanol solution of the 'stable' free radical, DPPH. The DPPH screening assay (despite its limitations) is a rapid technique for screening the radical scavenging activity of crude extracts from plants (or mixtures of compounds), foods, isolated compounds from natural sources and pure synthetic compounds, hence a commonly employed testing method in antioxidant studies.

A freshly prepared DPPH solution in ethanol which shows a deep purple colour fades in the presence of an antioxidant (via reduction by hydrogen atom (or one electron) donating) into the yellow-coloured diphenylpicrylhydrazine which is measured spectrophotometrically at 517 nm [53].

The results of *in vitro* antioxidant activity (IC_{50} values) of **11′**, hexane extract and fraction 10 in comparison with the reference antioxidant ascorbic acid are depicted in Fig. 6. From the results, it is noticed that the tested samples showed weak radical scavenging activity with IC_{50} values of 2.37 ± 0.08, 0.541 ± 0.032 and 0.353 ± 0.022 mg/mL for **11′**, fraction 10 and hexane extract, respectively. Among them, compound **11′** exhibited the least activity. This indicates that the chemical constituents in the crude hexane extract and fraction 10 are more potent in free radical scavenging compared to the isolated xanthene compound, probably due to the additive combination of the active constituents in the fraction and extract. However, the test samples exhibited weaker activity than the standard ascorbic acid, with IC_{50} value of 0.018 ± 0.003 mg/ml.

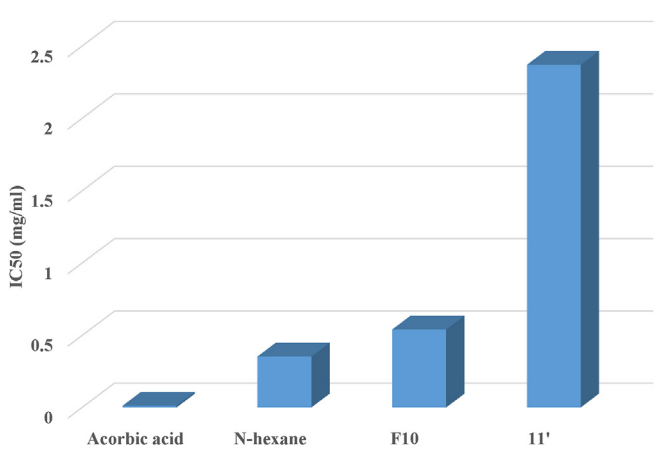

Fig. 6. IC_{50} (concentration required for 50% inhibition) values for DPPH radical scavenging activity of compound **11'**in comparison with hexane extract, fraction10 and the standard antioxidant AA.

3.4. Theoretical studies using DFT method

The accuracy of predicted geometric and electronic properties is a function of the quality of the optimized molecular structure. To investigate these properties for the current molecule, the choice of computational method was carefully made. For this purpose, an analytic procedure which includes a step-by-step geometry optimization using different basis functions in their increasing order was employed. This method permits the calculation of $\delta_{M(SUM)}$, the absolute difference between the computed and X-ray-determined bond lengths, and compare its value to the total energy of the molecule (E_M) as giving by each of the basis sets considered (Tables 1S and 2S, (see Supplementary data)). The primary conditions for attaining the 'equilibrium geometry' and which must be satisfied include, $\delta_{M(SUM)} \rightarrow 0$ as $E_M \rightarrow -\infty$. The closest basis to satisfying these conditions among those considered are the correlation-consistent polarized valence double zeta (cc-pVDZ) and the 6–311++G(d,p) basis sets (Table 3), as other higher-level basis sets armed with more diffuse and polarized functions could not be used due to the limited memory capacity of the computer system employed. The relationship between $\delta_{M(SUM)}$ and E_M has been graphically and pictorially represented in Fig. 7A, with the red and green arrows pointing in the appropriate directions. It then obviously indicates that none of these two prospective basis sets could explicitly satisfy both these conditions, i.e. $\delta_{M(SUM)} \rightarrow 0$ as $E_M \rightarrow -\infty$ simultaneously. What was observed is that cc-pVDZ satisfied the condition $\delta_{M(SUM)} \rightarrow 0$ while 6–311++G(d,p) satisfied the condition $E_M \rightarrow -\infty$ (Table 3 and Fig. 7A). These results are unconventional, as it would be expected that the basis with the lowest $\delta_{M(SUM)}$ automatically gives the lowest E_M value and vice-versa. Nonetheless, the secondary condition $|E_M|/\delta_{M(SUM)} \rightarrow \infty$, was best

Table 3
Total energy (E_M), $_{(SUM)}$ values and minimization coefficients per basis set.

Basis set	Total energy (E_M)/a.u.	$\delta_{M(SUM)}$ /Å	μ_M/a.u. Å^{-1}	% Rel. error per basis
6-31G	−1078.19	0.5202	2072.64	36.3
6-311G	−1078.43	0.4811	2241.60	33.7
6-311++G	−1078.45	0.4799	2247.23	33.5
[a]6-311++G(d,p)	−1078.76	0.4259	2532.91	29.3
[a]cc-pVDZ	−1078.54	0.3839	2809.42	26.6
LanL2DZ	−1078.31	0.6892	1564.58	48.0
SDD	−1078.31	0.6908	1560.96	48.1
Ideal	–	0.0000	5543.40	0.0

[a] E_M and $\delta_{M(SUM)}$ values do not conform.

Table 4
Experimental and Theoretical Wavenumbers and Band Assignments for compound 11.

Calculated (cm^{-1})	Experimental (cm^{-1})	Band assignments[a]
2979–2956	2956	$\upsilon_{as}CH_2$
2923–2921	2931	$\upsilon_{s}CH_2$
2898–2893	2854	υC-H
1693–1659	1666	υC = O
1611	1612	υC = C
1482	1464	δ C–H (CH_3)
1380	1381	δ C–H (CH2, CH3)
1214	1200	υC-O
1088–1082	1062	υC-O
758	750	γC-H (Ar)

[a] υ, stretching; δ, in-plane bending; γ, out-of-plane bending.

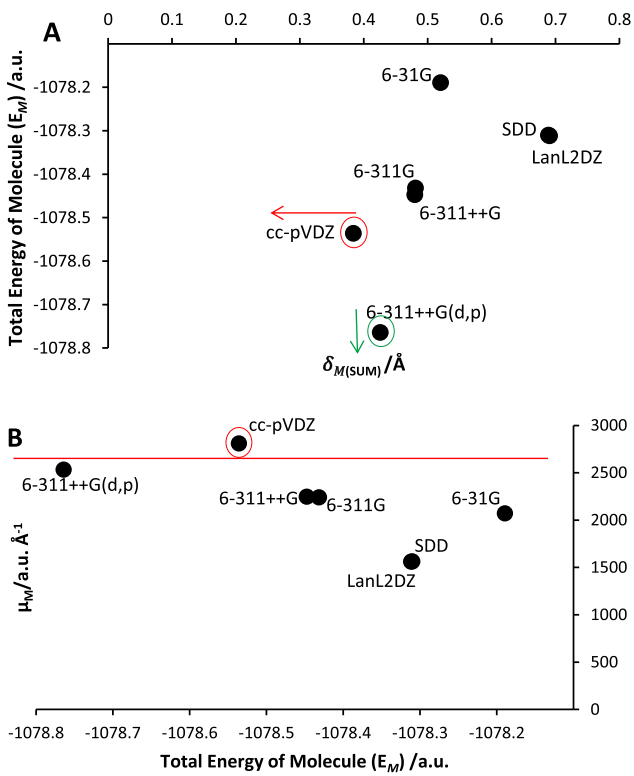

Fig. 7. (**A**) Energy gradient and (**B**) Minimization coefficient profiles.

satisfied by cc-pVDZ (Fig. 7B), and this warranted its use as the basis set for this investigation. The values of $|E_M|/\delta_{M(SUM)}$, i.e. μ_M, and the values of the relative error per basis set have been summarized in Table 3 with cc-pVDZ shown to give the least relative error value. The presence of H_2O molecule, H_3O^+ and Cl^- ions in the studied sample could explain why the calculated geometrical data deviate significantly from the experimental data (Table 2S (see Supplementary data)).

To confirm the suitability of cc-pVDZ for this study, the $\mu_M/\delta_{M(SUM)}$ data were fitted to Equation (3) (Fig. 8):

$$\mu_M = \mu_0 e^{-k\delta_{M(SUM)}} \quad (3)$$

where μ_0 is the minimization coefficient of the 'ideal' basis set for which $\delta_{M(SUM)} \rightarrow 0$, and has been extrapolated to be 5543.40 a.u. Å^{-1} (Fig. 8), k is any constant whose significance is not yet known, but

Table 5
Experimental and theoretical ^{13}C and ^{1}H chemical shifts (ppm) for the compound **11**.

Atom	Experimental (ppm)	Calculated, gas phase (ppm)
C1, C13	164.0	158.1, 157.8
C2, C12	37.0	29.0, 28.9
C3, C11	20.3	22.8, 24.2
C4, C10	27.2	37.7, 38.2
C5, C9	196.8	188.7, 189.1
C6, C8	116.9	117.7, 118.3
C7	31.3	34.9
C14	146.5	138.3
C15, C19	128.1	122.5, 128.4
C16, C18	126.4	119.6, 123.3
C17	146.5	141
C20	33.6	38.3
C21, C22	23.9	25.9, 25.7
H2, H12	2.64	2.61, 2.64
H3, H11	2.01	2.13, 2.16
H4, H10	2.40	2.38, 2.33
H7	4.78	4.49
H15, H19	7.05	6.86, 6.87
H16, H18	7.18	7.56, 7.11
H20	2.81	2.86
H21, H22	1.18	1.28, 1.30

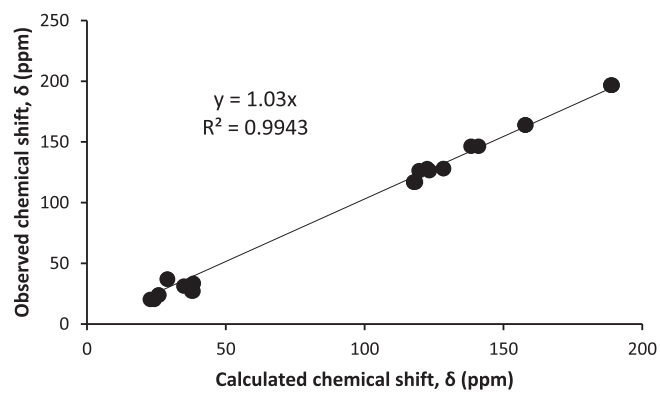

Fig. 9. Correlation plot showing the level of agreement between experiment and theory (only ^{13}C was used here).

tentatively, it has been interpreted as the number of basis functions that have overlapping $\delta_{M(SUM)}$ values. Here, 1.849 has been obtained for k, which is approximately 2, and coincidentally the number of basis functions found with overlapping $\delta_{M(SUM)}$. It is now obvious from Fig. 8 that the closest basis to the 'ideal' is the cc-pVDZ. Hence, subsequent calculations such as the vibrational frequencies to classify the optimized structure as local minimum or transition

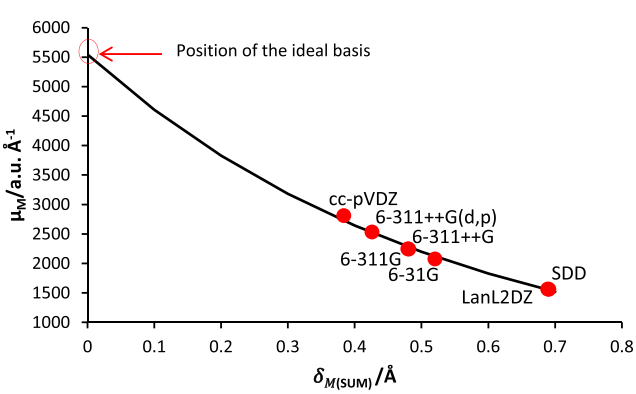

Fig. 8. Graph showing the gap between the methods employed and the ideal method.

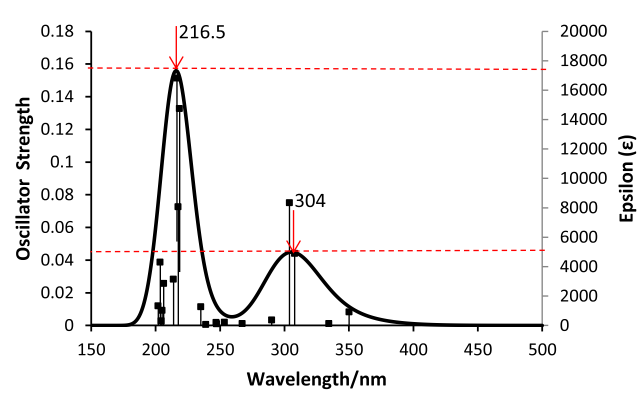

Fig. 10. Calculated electronic absorption spectrum (at B3LYP/cc-pVDZ level).

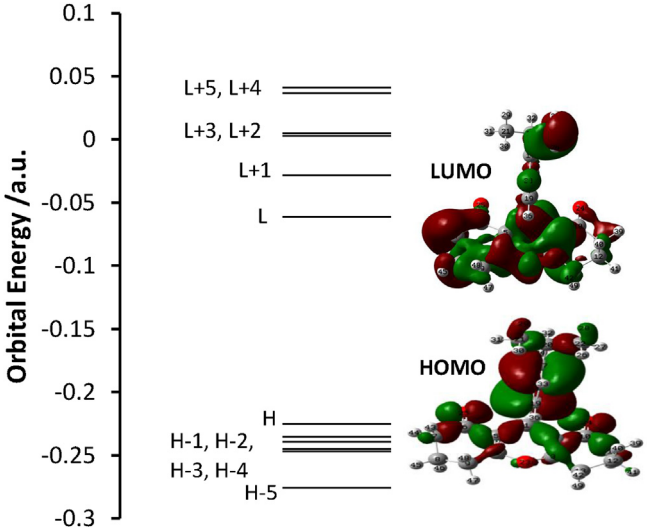

Fig. 11. Some of the orbital energy levels involved in the electronic transitions.

state, and the time-dependent self-consistent field (TD-SCF), for $N = 20$ states, to understand the electronic absorption behavior of the molecule were performed at the cc-pVDZ level. However, the B3LYP/cc-pVDZ level was found too computationally expensive to generate the NMR data, due to the limited memory capacity of the computer system employed. The ^{1}H and ^{13}C NMR were then finally obtained at the B3LYP/6-31G//B3LYP/cc-pVDZ level of theory.

The X-ray crystallography and the calculated structures of the studied molecule **(11)** are presented in Fig. 4. The removal of the hydrogen atoms in the computed structure (Fig. 4B) was intentional for clarity purpose. The vibrational analysis confirmed the stability of the adopted geometry (Fig. 4B), as no first order saddle point was found. The experimental X-ray data are mostly well reproduced by the B3LYP/cc-pVDZ (Tables 1S and 2S (see Supplementary data)), and as such, predicted properties based on this geometry are closest to the experimental values.

The theoretical and experimental IR frequency and NMR data of the 9-[4-(propan-2-yl)phenyl]-3,4,5,6,7,9-hexahydro-1*H*-xanthene-1,8(2*H*)-dione (**11**) are presented with band and chemical shifts assignments in Tables 4 and 5 respectively. The calculated data were found to compare reasonably well with the experiment. For example. Fig. 9 shows the degree of correlation of the NMR data, and confirms the appropriateness of the adopted theoretical method. The observed difference between the experiment and theory can be explained from the solvent effects perspective, since the IR and NMR data were obtained in the gas phase. Detailed comparisons of experimental and theoretical IR or NMR data of similar organic compounds are available in the literature [54–56].

Fig. 10 shows the electronic absorption bands as a function of the oscillator strength (f) and the absorption coefficient (ε) obtained at the B3LYP/cc-pVDZ level. It is a common knowledge that absorption bands are produced from the effects of several molecular orbital (MO) interactions or mixing [57,58]. The calculation revealed that the maximum absorption wavelength (λ_{max}), found to be 216.5 nm, results mainly from the transitions between the highest occupied molecular orbital (HOMO) and the higher-level lowest unoccupied molecular orbitals (LUMOs), i.e. (L+2) and (L+3). HOMO and LUMO are denoted by H and L respectively. The percentage contributions of H → (L+2) and H → (L+3) to λ_{max} are found to be 26.13 and 46.48% respectively. A snippet of the contributions to the absorption

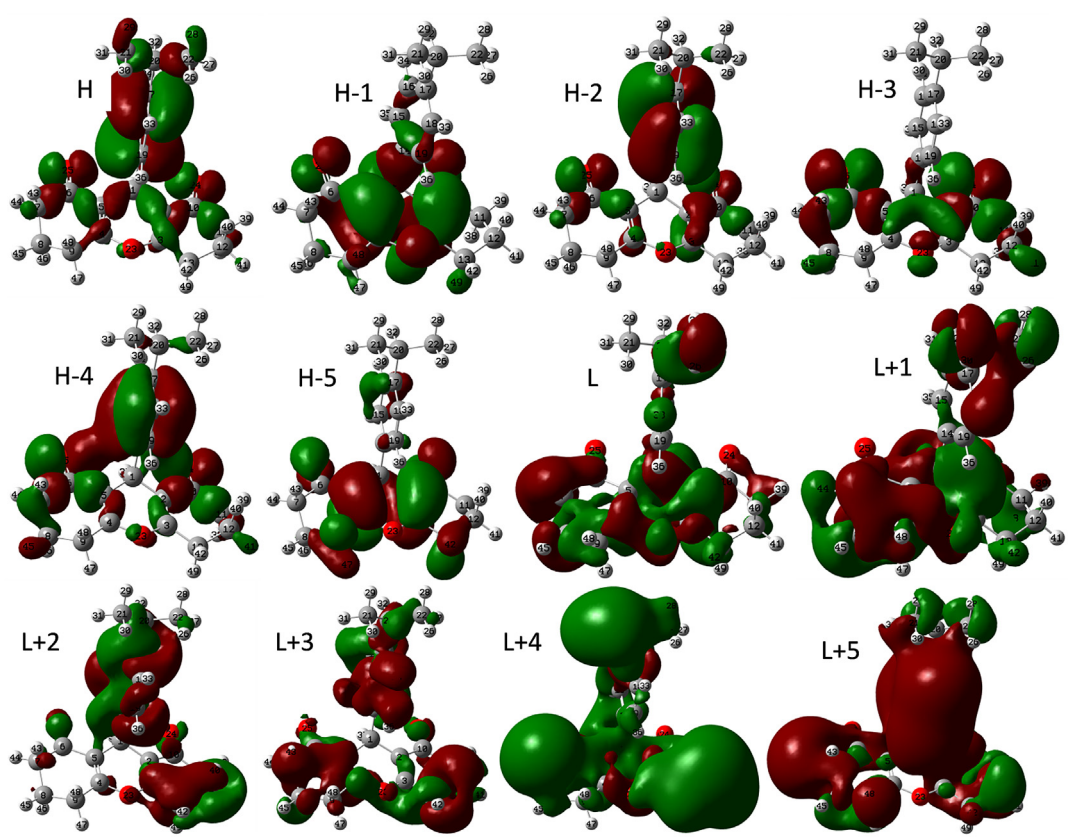

Fig. 12. The molecular orbital diagrams of the electronic levels.

at this wavelength, λ_{max}, was found also from (H-2) → (L+3) and (H-4) → (L+2) MOs with 13.60 and 13.79% contributions respectively. The transitions giving rise to the λ_{max} corresponds to the n → σ* type, since it has the highest energy compared to π → π* and n → π* transitions, which are the other possible transitions that may be found in this molecule. The band at 304 nm (Fig. 10), results from the contributions of the transitions from (H-3) → L (24.64%) and (H-1) → L (75.36%) MOs, and corresponds to π → π* transitions. The calculated energy levels and the molecular orbitals presented in Figs. 11 and 12 respectively may be used to explain some of these MO transitions. It is obvious from Fig. 8 that the electron density distribution in the H, (H-2) and (H-4) MOs are mostly concentrated on the cumene fragment, which to a good approximation, shows that their symmetry structures are closely similar. The similarity of these structures places them on the same geometrical pedestal to absorb radiation of appropriate wavelengths and become excited into higher-level MOs such as the (L+2) and (L+3), which also has similar electron distribution patterns as them (Figs. 11 and 12). Contributions of H → L transition to the spectrum was found only in the absorptions at 308 and 350 nm, which are unsurprisingly weak (Fig. 11) [59], and corresponds to a n → π* transition. The calculated HOMO-LUMO energy (0.164 a.u. ≈ 431 kJ mol^{-1}) may be too high for applications requiring spontaneous photo-induced electron transfer processes, and this may explain why the DPPH radical scavenging activity of the molecule is low.

4. Conclusions

In the present study, we report the isolation of a 1,8-xanthenedione from the seeds of *Garcinia kola* and its characterization by FTIR, NMR and single crystal X-ray diffraction crystallography. The ^{1}H, ^{13}C and FTIR spectral results are in line with the proposed structure. Comparison of the X-ray bond length data of the target molecule, $C_{22}H_{24}O_3$, with the DFT calculation is good. The theoretical IR frequency and NMR data were found to compare reasonably well with the experimental values. A time-dependent density functional theory (TD-DFT) method has been used to describe the electronic absorption behavior of the $C_{22}H_{24}O_3$ xanthenedione derivative. The λ_{max} at 216.5 nm corresponds to a n → σ* transition, resulting from contributions from H → (L+2), H → (L+3), (H-2) → (L+3) and (H-4) → (L+2) interactions. The absorption at 304 nm corresponds to a π → π* transition which results from contributions from (H-3) → L and (H-1) → L interactions. Contributions of H → L interaction to the absorptions at 308 and 350 nm are weak, and correspond to an n → π* transition. The calculated HOMO-LUMO energy (0.164 a.u. ≈ 431 kJ mol^{-1}) may be too high for applications requiring spontaneous photo-induced electron transfer processes, and this may explain why the DPPH radical scavenging activity of the molecule is low. The results of the X-ray structural analysis of compound **(11′)** show that the molecular packing of the molecule is stabilized by weak C=O- - –H, C–H- - -O—H- - –Cl intermolecular interactions as well as some weak C–H ⋯ π and intramolecular interactions. The compound $C_{22}H_{24}O_3$ was found to display weak DPPH radical scavenging activity. This is the first time a xanthenedione derivative is reported from the seed of *Garcinia kola*.

Acknowledgments

JPJ acknowledges the NSF–MRI program (grant No. CHE-1039027) for funds to purchase the X-ray diffractometer.

Appendix A. Supplementary data

Supplementary data related to this article can be found at http://dx.doi.org/10.1016/j.molstruc.2017.05.026.

References

[1] J. Hutchinson, J.M. Dalziel, Flora of West Tropical Africa, second ed., vol. 1, HMSO, London, 1956, p. 295.
[2] J.M. Dalziel, The Useful Plants of West Tropical África, Crown Agents for the Colonies, London, 1937.
[3] M.M. Iwu, Handbook of African Medicinal Plants, CRC Press Inc., Boca Raton, 1993, pp. 223–224.
[4] S.K. Adesina, Z.O. Gbile, O.A. Odukoya, D.D. Akinwusi, H.C. Illoh, A.A. Yeola, Survey of Indigenous Useful Plants of West Africa with Special Emphasis on Medicinal Plants and Issues Associated with Management, The United Nations Programme on Natural Resources in Africa, second ed., 1995, pp. 84–85.
[5] P.E. Ajebesone, J.O. Aina, J. Food Technol. Afr. 9 (2004) 13–16.
[6] E.S. Ayensu, Medicinal Plants of West Africa, Reference Publ. Inc, Algonac, Michigan, 1978, p. 162.
[7] J.F. Akoachere, R.N. Ndip, E.B. Chenwi, L.M. Ndip, T.E. Njock, D.N. Anong, East Afr. Med. J. 79 (2002) 588–592.
[8] D.A. Akinpelu, M.F. Adegboye, O.A. Adeloye, A.I. Okoh, Biol. Res. 41 (2008) 277–287.
[9] S.B.I. Olaleye, E.O. Farombi, E.A. Adewoye, B.V. Owoyele, S.A. Onasanwo, R.A. Elegbe, Afr. J. Biomed. Res. 3 (2000) 171–174.
[10] C.O. Nwaehujor, R.I. Udegbunam, J.O. Ode, S.O. Udegbunam, J. Korean Soc, Appl. Biol. Chem. 58 (2015) 91–96.
[11] B. Konziase, J. Ethnopharmacol. 172 (2015) 214–218.
[12] E.O. Farombi, O.O. Akanni, G.O. Emerole, Pharm. Biol. 40 (2002) 107–116.
[13] T. Okoko, Food Chem. Toxicol. 47 (2009) 2620–2623.
[14] E.O. Farombi, O. Owoeye, Int. J. Environ. Res. Publ. Health 8 (2011) 2533–2555.
[15] M.K. Tchimene, A.O. Anaga, C.E.C. Ugwoke, O.J. Onoja, C.O. Ezugwu, C. Okunji, M.M. Iwu, Int. J. Curr. Microbiol. App. Sci. 5 (2016) 317–322.
[16] C.O. Okunji, M.M. Iwu, Fitoterapia 62 (1991) 74–76.
[17] O.A. Adaramoye, V.O. Nwaneri, K.C. Anyanwu, E.O. Farombi, G.O. Emerole, Clin. Exp. Pharmacol. Physiol. 32 (2005) 40–46.
[18] N. Ralebona, C.R. Sewani-Rusike, B.N. Nkeh-Chungag, Afr. J. Pharm. Pharmacol. 6 (2012) 1077–1082.
[19] M.M. Iwu, O.A. Igboko, C.O. Okunji, S. Tempesta, J. Pharm. Pharmacol. 42 (1990) 290–292.
[20] O.O. Azu, A.A. Osinubi, C.C. Noronha, A.O. Okanlawon, West Afr. J. Anat. 8 (2005) 141–149.
[21] K. Omage, O.G. Idokpesi, J.S. Josiah, S.E. Uhunmwangho, O.K. Ajeigbe, Res. J. Biol. Sci. 5 (2010) 647–664.
[22] O.O. Adegbehingbe, S.A. Adesanya, T.O. Idowu, O.C. Okimi, O.A. Oyelami, E.O. Iwalewa, J. Orthop. Surg. Res. 3 (2008) 34.
[23] S. Kumar, S. Sharma, S.K. Chattopadhyay, Fitoterapia 89 (2013) 86–125.
[24] S. Baggett, P. Protiva, E.P. Mazzola, H. Yang, E.T. Ressler, M.J. Basile, I.B. Weinstein, E.J. Kennelly, J. Nat. Prod. 68 (2005) 354–360.
[25] J.T. Lyles, A. Negrin, S.I. Khan, K. He, E.J. Kennelly, Planta Med. 80 (2014) 676–681.
[26] Y. Sakagami, M. Iinuma, K.G. Piyasena, H.R. Dharmaratne, Phytomedicine 12 (2005) 203–208.
[27] M. Iinuma, H. Tosa, T. Tanaka, S. Kanamaru, F. Asai, Y. Kobayashi, K. Miyauchi, R. Shimano, Biol. Pharm. Bull. 19 (1996) 311–314.
[28] G. Gopalakrishnan, B. Banumathi, G. Suresh, J. Nat. Prod. 60 (1997) 519–524.
[29] S. Sang, M.H. Pan, X. Cheng, N. Bai, R.E. Stark, R.T. Rosen, S.Y. Lin-Shiau, J.K. Lin, C.T. Ho, Tetrahedron 57 (2001) 9931–9938.
[30] S. Sang, C.H. Liao, M.H. Pan, R.T. Rosen, S.Y. Lin-Shiau, J.K. Lin, C.T. Ho, Tetrahedron 58 (2002) 10095–10102.
[31] D.H. Trinh, L.D. Ha, P.T. Tran, L.-H.D. Nguyen, Nat. Prod. Commun. 9 (2014) 1737–1740.
[32] K. Terashima, T. Shimamura, M. Tanabayashi, M. Aqil, J.A. Akinniyi, M. Niwa, Heterocycles 45 (1997) 1559–1566.
[33] D.E. Okwu, F.N.I. Morah, J. Appl. Sci. 7 (2007) 306–309.
[34] A.M.L. Seca, S.B. Leal, D.C.G.A. Pinto, M.C. Barreto, A.M.S. Silva, Molecules 19 (2014) 8317–8333.
[35] J. Chen, J. Shi, C.-G. Yan, Chem. Res. Chin. Univ. 27 (2011) 49–53.
[36] O.V. Dolomanov, L.J. Bourhis, R.J. Gildea, J.A.K. Howard, H. Puschmann, J. Appl. Cryst. 42 (2009) 339–341.
[37] L. Palatinus, G. Chapuis, J. Appl. Cryst. 40 (2007) 786–790.
[38] G.M. Sheldrick, Acta Cryst. A64 (2008) 112–122.
[39] C.-W. Chen, C.-T. Ho, J. Food Lipids 2 (1995) 35–46.
[40] M.J. Frisch, G.W. Trucks, H.B. Schlegel, G.E. Scuseria, M.A. Robb, J.R. Cheeseman, J.A. Montgomery Jr., T. Vreven, K.N. Kudin, J.C. Burant, J.M. Millam, S.S. Iyengar, J. Tomasi, V. Barone, B. Mennucci, M. Cossi, G. Scalmani, N. Rega, G.A. Petersson, H. Nakatsuji, M. Hada, M. Ehara, K. Toyota, R. Fukuda, J. Hasegawa, M. Ishida, T. Nakajima, Y. Honda, O. Kitao, H. Nakai, M. Klene, X. Li, J.E. Knox, H.P. Hratchian, J.B. Cross, V. Bakken, C. Adamo, J. Jaramillo, R. Gomperts, R.E. Stratmann, O. Yazyev, A.J. Austin, R. Cammi, C. Pomelli, J.W. Ochterski, P.Y. Ayala, K. Morokuma, G.A. Voth, P. Salvador, J.J. Dannenberg, V.G. Zakrzewski, S. Dapprich, A.D. Daniels, M.C. Strain, O. Farkas, D.K. Malick, A.D. Rabuck, K. Raghavachari, J.B. Foresman, J.V. Ortiz, Q. Cui, A.G. Baboul, S. Clifford, J. Cioslowski, B.B. Stefanov, G. Liu, A. Liashenko, P. Piskorz, I. Komaromi, R.L. Martin, D.J. Fox, T. Keith, M.A. Al-

Laham, C.Y. Peng, A. Nanayakkara, M. Challacombe, P.M.W. Gill, B. Johnson, W. Chen, M.W. Wong, C. Gonzalez, J.A. Pople, In Gaussian 03, Revision E.01, Gaussian, Inc., Wallingford CT, 2004.
[41] (a) A.D. Becke, J. Chem. Phys. 98 (1993) 5648–5652;
(b) A.D. Becke, J. Chem. Phys. 96 (1992) 2155–2160;
(c) A.D. Becke, J. Chem. Phys. 97 (1992) 9173–9177.
[42] C. Lee, W. Yang, R.G. Parr, Phys. Rev. B 37 (1988) 785–789.
[43] S.-H. Ke, H.U. Baranger, W. Yang, J. Chem. Phys. 127 (2007) 144107.
[44] A. Masunov, S. Tretiak, J. Phys. Chem. B 108 (2004) 899–907.
[45] T.K. Ghanty, S.K. Ghosh, J. Phys. Chem. A 107 (2003) 7062–7067.
[46] K. Sanusi, S. Khene, T. Nyokong, Opt. Mater. 37 (2014) 572–582.
[47] H.-T. Chen, J.-J. Ho, J. Phys. Chem. A 107 (2003) 7004–7012.
[48] K. Wolinski, J.F. Hilton, P. Pulay, J. Am. Chem. Soc. 112 (1990) 8251–8260.
[49] J.R. Cheeseman, G.W. Trucks, T.A. Keith, M.J. Frisch, J. Chem. Phys. 104 (1996) 5497–5509.
[50] B.F. Lira, J. Miller, A.M. Simas, P.F. Athayde-Filho, A. de F. Dias, R.O. Silva, V. Carlos de Oliveira, Ark. (vi) (2004) 12–21.
[51] D. Cremer, J.A. Pople, J. Am. Chem. Soc. 97 (1975) 1354–1358.
[52] F.H. Allen, O. Kennard, D.G. Watson, L. Brammer, A.G. Orpen, R. Taylor, J. Chem. Soc. Perkin Trans. 2 (1987) (1987) S1–S19.
[53] T. Yamaguchi, H. Takamura, T. Matoba, J. Terao, Biosci. Biotechnol. Biochem. 62 (1998) 1201–1204.
[54] U. Yadava, D.K. Gupta, M. Roychoudhury, J. Mol. Liq. 156 (2010) 187–190.
[55] B.K. Shukla, U. Yadava, M. Roychoudhury, J. Mol. Liq. 212 (2015) 325–330.
[56] U. Yadava, M. Singh, M. Roychoudhury, Comput. Theor. Chem. 977 (2011) 134–139.
[57] P. Douglas, H.D. Burrows, R.C. Evans, Foundations of photochemistry: a background on the interaction between light and molecules, in: R.C. Evans, et al. (Eds.), Applied Photochemistry, Springer Science+Business Media Dordrecht, 2013, pp. 1–88.
[58] J.A. Weinstein, Inorganic photochemistry, in: R.C. Evans, et al. (Eds.), Applied Photochemistry, Springer Science+Business Media Dordrecht, 2013, pp. 105–148.
[59] S. Kumar, Spectroscopy of Organic Compounds, 2006. Available at: www.uobabylon.edu.iq/eprint/publication_11_8282_250.pdf.